# Influence of the meandering channel geometry on the thermo-hydraulic performances of an intensified heatexchanger/reactor

Zoé Anxionnaz-Minvielle, Michel Cabassud, Christophe Gourdon, Patrice Tochon

**HAL Id: hal-00905419**

**https://hal.science/hal-00905419**

Submitted on 18 Nov 2013

# Influence of the meandering channel geometry on the thermo-hydraulic performances of an intensified heat exchanger/reactor

Zoé Anxionnaz-Minvielle [a,*], Michel Cabassud [b], Christophe Gourdon [b], Patrice Tochon [a]

[a] CEA, LITEN, LETH, 17 rue des Martyrs, 38054 Grenoble, France
[b] University of Toulouse, Laboratoire de Génie Chimique, UMR 5503, CNRS/INPT/UPS, 31432 Toulouse, France

## ABSTRACT

In the global context of process intensification, heat exchanger/reactors are promising apparatuses to implement exothermic chemical syntheses. However, unlike heat exchange processes, the implementation of chemical syntheses requires to control the residence time to complete the chemistry. A way to combine the laminar regime (i.e. enough residence time) with a plug flow and the intensification of both heat and mass transfers is the corrugation of the reaction path.

In this work, the experimental set-up is based on plate heat exchanger/reactor technology. 7 milli-channel corrugated geometries varying the corrugation angle, the curvature radius, the developed length, the hydraulic diameter and the aspect ratio have been designed and experimentally characterized (heat transfer, mixing times, pressure drops, RTD). The objectives were to assess their respective performances to derive some correlations depending on the channel design.

The results confirmed the benefits of the reaction channel corrugation. Heat and mass transfers have been intensified while maintaining a plug flow behaviour in the usually laminar flow regime. Moreover, whatever the meandering channel's curvature radius, the results highlighted the relevance of considering the Dean number as the scale-up parameter. This dimensionless number, more than the Reynolds number, seems to govern the flow in the wavy channels.

## 1. Introduction

In the global context of process intensification, defined by Stankiewicz and Moulijn [1] as "any chemical engineering development that leads to a substantially smaller, safer, cleaner and more energy-efficient technology", heat exchanger/reactors are promising apparatuses [2,3]. Indeed, by combining a reactor and a heat exchanger in only one unit the heat generated (or absorbed) by the reaction is removed (or supplied) much more rapidly than in a classical batch reactor. As a consequence, heat exchanger/reactors may offer better safety (by a better thermal control of the reaction), better selectivity (by a more controlled operating temperature) and by-products reduction (in case of temperature-dependent secondary reaction for instance).

The main interesting ways to intensify heat and mass transfers in heat exchanger/reactors are to insert 3D elements like metallic foams or fins [4–6] or to structure the flow path (2D or 3D) [7–13]. Such apparatuses have to address many points in terms of performances, but also in terms of polyvalence (the technology should not be dedicated to only one application), flexibility (to easily switch from one flow regime to another), competitiveness (too complex geometries lead to too high manufacturing and operating costs) and scale-up (performances have to be maintained during the scale-up procedure).

To optimize the heat exchanger/reactor performances vs. the investment capacity, the first step is to characterize the flow behaviour and the transfer mechanisms [8,14]. This is one of the objectives of this work. A 2D-structured millimetric and meandering process channel is considered. Contrary to the flow in a straight channel, the streamlines in a corrugated flow are not parallel to the flow axis. The centrifugal force encountered in each bend and the imbalance between this force and the pressure gradient generate counter-rotating vortices in the channel cross section. W.R. Dean [15] was the first to solve the flow solution in a curved duct. He defined the Dean number, De, which takes into account the secondary loops generated in a corrugated channel:

$$De = Re \times \sqrt{\frac{d_h}{R_c}} \tag{1}$$

* Corresponding author. Tel.: +33 0438783567; fax: +33 0438785161.
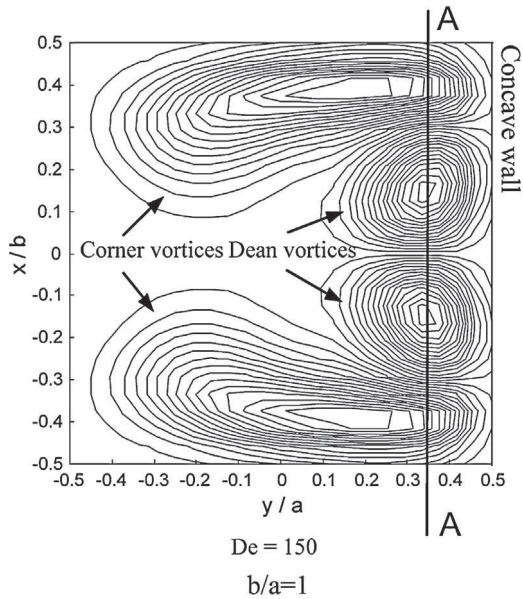  *E-mail address:* zoe.minvielle@cea.fr (Z. Anxionnaz-Minvielle).

**Fig. 1.** Visualization of the secondary loops in a square duct cross section [16].

Re is the Reynolds number,

$$Re = \frac{\rho \times u \times d_h}{\mu} \tag{2}$$

$\rho$, $\mu$ and $u$ are respectively the flow density (kg m$^{-3}$), viscosity (Pa s) and velocity (m s$^{-1}$). $d_h$ is the channel hydraulic diameter (m) and $R_c$ is the curvature radius (m).

An increase of the Dean number tends to move the axial velocity peak from the centre to the outward duct wall. Above a critical value of the Dean number, because of the flow instability, two additional vortices appear. They are called the Dean vortices. Fig. 1 illustrates this flow phenomenon.

The critical Dean number ranges between 100 and 250 according to the employed Dean vortices detection method [16–18]. Downstream each bend, the flow tends to a laminar flow in the straight length. By alternating the corrugations, the flow instabilities are reactivated in each bend which promotes the radial homogenization of the velocity, temperature and momentum fields [19].

On the other hand, this expected gradients homogenization has to be balanced with a pressure drop increase. The goal of this work is thus to optimize the corrugated channel geometry in order to intensify the heat and mass transfers while getting a low Reynolds number flow. This last point is required to have reasonable residence time (to complete the chemistry) and low pressure drop.

Moreover to expect a future industrialization of heat exchanger/reactor technologies, the scalability is another major step to study. Indeed, during the scale-up procedure, each similitude law (hydrodynamics, chemistry, geometry,...) should be verified in order to maintain the performances. However each law is characterized by its own invariant parameter (time, length,...) and it is often impossible to verify the principle of similitude:

$$G_{mock-up} = k \times G_{pilot}, \text{ with } k \text{ a constant parameter} \tag{3}$$

It is thus required to characterize the effect of the scale-up on the performances of our system. The 2nd objective of this work is then to deduce rules and correlations which will be used to predict the performances of the meandering channel at a pilot scale.

In the present work, a plate-type heat exchanger/reactor, including one process plate and one cooling plate, has been studied. On each plate, a wavy milli-channel has been mechanically etched. This work aims at characterizing the flow performances in several geometries in terms of residence time distribution,
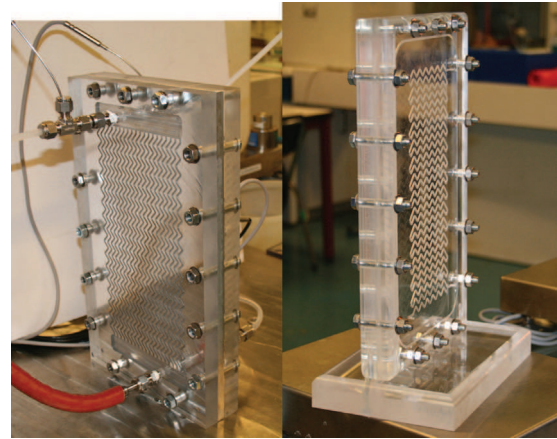


**Fig. 2.** View of the process channels without the utility plate (right side) and view of the utility channels ((left side).

mixing times, heat transfer and pressure drops. Both the influence of the channel geometry and the influence of the channel characteristic sizes (hydraulic diameter and aspect ratio) have been studied. Seven geometries have been considered and a mock-up has been built for each one.

## 2. Materials and methods

### 2.1. Experimental mock-ups

The mock-ups are made of three plates: a cooling plate sandwiched between a closing plate and a 'process plate' in which the reactants are flowing co-currently. The cooling plate is a 7 mm thickness aluminium plate with a high thermal conductivity ($\lambda = 247$ W m$^{-1}$ K$^{-1}$). It is used during thermal experiments and is removed for the hydrodynamic characterizations. Both the closing and 'process' plates are made of PolyMethylMethAcrylate (PMMA), whose thermal conductivity, coupled to a thickness of 20 mm, is low enough to avoid thermal losses ($\lambda = 0.19$ W m$^{-1}$ K$^{-1}$ and $\lambda/e = 8.5$ W m$^{-2}$ K$^{-1}$; negligible in comparison with the local heat transfer coefficients). The transparency of these plates is necessary in order to visualize the flow in the channel during mixing experiments. To test various channel designs, the mock-ups have to be easily and quickly implemented. As a consequence, each plate is etched in the laboratory with a numerically controlled milling machine. Then, the plates are assembled with 16 clamping screws for the thermal experiments (see Fig. 2), or chemically bonded for the hydrodynamic tests.

Each mock-up is connected to a test bench equipped with 2 magnetic drive pumps (Verder, 0–5 and 0–10 L h$^{-1}$), three mass flow metres (Micromotion), a differential pressure measuring transducer (Rosemount, 0–5 bars), 12 temperature probes (Pt100 and thermocouples), two spectrophotometers (AvaSpec 2048, AvaLight DHc and In-line flow cells Avantes) and a syringe pump. Experimental data (temperature, flowrate, pressure and absorbance) are recorded by an on-line data storage system.

### 2.2. Geometrical parameters of the wavy channels

Two main challenges have to be addressed when structuring the wavy channels:

- How can *a plug flow* and *a sufficient residence time* for the chemistry be combined?
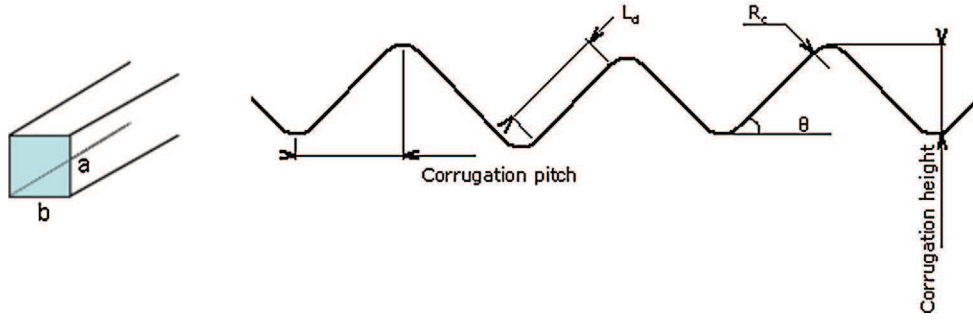
**Fig. 3.** Schematic view of the geometrical parameters.

- How can a *laminar flow* (in order to get a sufficient residence time and low pressure drop) and the *intensification* of mass and heat transfers be combined?

In order to optimize the geometry with respect to these criteria, the influence of the geometrical parameters on residence time distribution, mixing, thermal performances and pressure drops has been investigated in this work.

The geometrical parameters were chosen with regards to those commonly studied in the literature. Cheng et al. [20] and Fellouah et al. [16] studied the influence of both the curvature radius and the aspect ratio on the critical Dean number. The aspect ratio is defined as the ratio between the duct height and its width. Works about its influence on both the Nusselt number [21,22] and the friction factor [23] have also been done. Finally the effects of corrugation angle [24,25] and corrugation pitch [25,26] have been studied.

From these works, four parameters appear to be important (see Fig. 3): the aspect ratio, $a/b$ with $a$ and $b$ respectively the channel height and width; the curvature radius, $R_c$; the corrugation angle, $\theta$ and the straight length, $L_d$ which corresponds to the length between two bends. The corrugation pitch and the corrugation height both depend on the corrugation angle and the straight length.

The value of the curvature radius depends on the channel width as illustrated on the Fig. 4.

The channel width in Fig. 4 is equal to 4.02 mm. Three curvature radius values coexist. The curvature radius defined along the neutral axis equals 4 mm whereas the external curvature radius ($R_{c,e}$) and the internal curvature radius ($R_{c,i}$) are respectively equal to 6 and 2 mm. They are defined by:

$$R_{c,e} = R_c + \frac{b}{2} \qquad (4)$$

and

$$R_{c,i} = R_c - \frac{b}{2} \qquad (5)$$

with $b$ the channel width.

The Dean number is defined as $De = Re \times \sqrt{\frac{d_h}{R_c}}$. As a consequence, three different Dean numbers can be considered in the channel. The largest one, i.e. the one resulting from the smallest
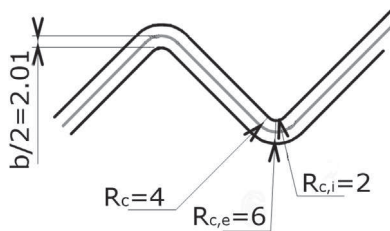
curvature radius (the internal curvature radius), will be named the internal Dean number, $De_i$.

In order to identify the influence of each parameter on the thermo-hydraulic performances, only one parameter varies from one mock-up to another. The geometrical data are given in Table 1 and Fig. 5 illustrates them.

The mock-up 'a' is made of 37 rows and 36 180° turning bends. 2 rows are illustrated in Fig. 5. Each row is 90 mm long. Then, from mock-up 'b' to mock-up 'g', only one parameter changes from a mock-up to another. As a consequence to understand the influence of each geometrical parameter, it is important to compare the right mock-ups. For instance, to study the influence of the curvature radius, only the performances of mock-ups 'd' and 'e' will be compared. The hydraulic diameter of mock-up 'g' (4 mm) has been chosen so as to have a range of Reynolds number in common with the 2 mm mock-ups without any major change of the pump or flow metre equipment.

### 2.3. Experimental characterizations

The mock-ups have been characterized in terms of pressure drops, Residence Time Distribution (RTD), thermal performances and mixing [27]. These characterizations aim at both studying the flow behaviour according to the geometrical parameters and correlating the performances to a scale-up parameter.

Pressure drops are measured with a differential pressure sensor. Its measurement range varies from 0 to 5 bar with an accuracy
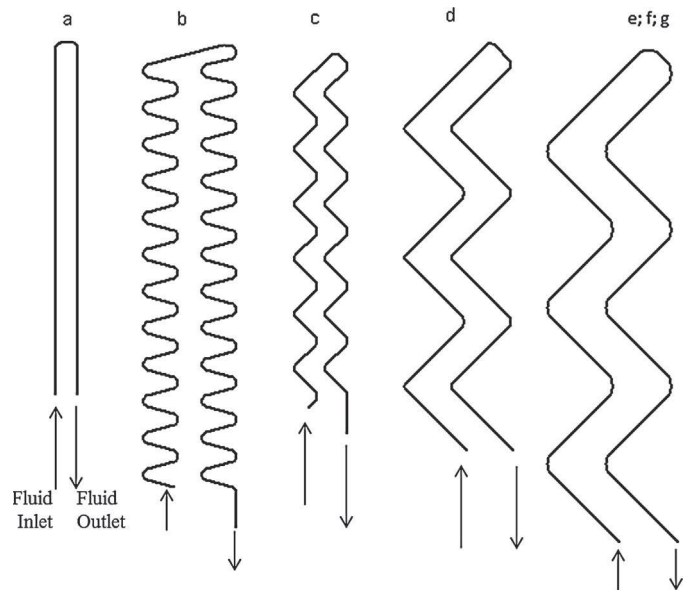


**Fig. 4.** Schematic view of the corrugated channel of 4.02 mm width.



**Fig. 5.** Schematic view of 2 rows of the corrugated channels.

**Table 1**
Geometrical data of the corrugation parameters.

| Mock-up n° | a/b | $d_{h,eq}$ | θ | $R_{c,i}$ (mm) | $L_d$ (mm) | $L_{tot}$ (m) | $V_{tot}$ (cm³) | $N_b/L$ (bends/m) |
|---|---|---|---|---|---|---|---|---|
| a | 1 (2/2 mm) | 2 | – | – | 90 | 3,6 | 13,6 | 20 |
| b | 1 (2/2 mm) | 2 | 75° | 0.5 | 6.94 | 5.0 | 20.0 | 90 |
| c | 1 (2/2 mm) | 2 | 45° | 0.5 | 6.94 | 3.5 | 14.0 | 106 |
| d | 1 (2/2 mm) | 2 | 45° | 0.5 | 20.28 | 3.5 | 14.0 | 44 |
| e | 1 (2/2 mm) | 2 | 45° | 3 | 20.28 | 3.4 | 13.6 | 38 |
| f | 0.5 (2/4 mm) | 2.67 | 45° | 3 | 20.28 | 3.4 | 27.2 | 38 |
| g | 1 (4/4 mm) | 4 | 45° | 2 | 20.28 | 3.4 | 54.4 | 38 |

of ±5%. Pressure probes are set at the inlet and the outlet of the mock-ups where temperature sensors are also connected. The temperature is, indeed, an important data to assess the fluid properties (density and viscosity). The working fluids are distilled water and 67%w. glycerol. From the experimentally measured pressure drop, the Darcy coefficient, Λ, is assessed according to the following expression:

$$\Lambda = \frac{\Delta P}{\frac{L}{d_h} \times \rho \times \frac{u^2}{2}} \quad (6)$$

with ρ the fluid density (kg m⁻³), u its velocity (m s⁻¹); L and $d_h$ respectively the length (m) and the hydraulic diameter (m) of the channel and ΔP the pressure drop (P a).

The thermal study is based on experiments which aim at cooling the fluid flowing in the process plate. Process fluid is distilled water heated at 75 °C whereas utility fluid is raw water at about 13 °C. For each experiment, the utility flowrate is set to 100 L h⁻¹ whereas the process flowrate varies from 1 to 15 L h⁻¹. In order to avoid temperature pinch, temperature is measured all along the channel: 6 temperature sensors are set between the inlet and the outlet of the process plate and 2 temperature sensors are set at the inlet and the outlet of the cooling plate. The temperature profile all along the process channel shows that between 40 and 60% of the total channel length is sufficient to exchange the heat duty. As a consequence, the thermal balances have been made between the process channel inlet and the first temperature sensor, which is located on the 2nd row (0.26 m from the inlet). From the measured temperature difference, ΔT, the exchanged thermal power, P(W), is assessed:

$$P = \dot{m} \times C_p \times \Delta T \quad (7)$$

$\dot{m}$ and $C_p$ are respectively the flowrate (kg s⁻¹) and the specific heat of the fluid (J kg⁻¹ K⁻¹).

The global heat transfer coefficient, U (W m⁻² K⁻¹), is then calculated with:

$$U = \frac{P}{A \times \Delta T_{ml}} \quad (8)$$

$\Delta T_{ml}$ is the logarithmic mean temperature difference and A the heat exchange area. As previously described, the channel is etched in a PMMA plate and closed with an aluminium plate. As a consequence the heat exchange area corresponds to the area in contact with the aluminium plate.

The Nusselt number is written as:
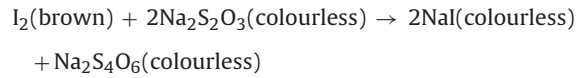
$$Nu = \frac{h_p \times d_h}{\lambda_p} \quad (9)$$

$d_h$ is the channel hydraulic diameter and $\lambda_p$ is the fluid thermal conductivity (W m⁻¹ K⁻¹). $h_p$ is the local heat transfer coefficient of the process fluid (W m⁻² K⁻¹) and is deduced from the following equation:s

$$\frac{1}{U \times A} = \frac{1}{h_p \times A_p} + \frac{e}{\lambda} + \frac{1}{h_u \times A_u} \quad (10)$$

e and λ are respectively the thickness and the thermal conductivity of the aluminium plate (W m⁻¹ K⁻¹). $h_u$ is the local heat transfer coefficient of the cooling side. It has been assessed to be 27 kW m⁻² K⁻¹ in our geometry. This value is high enough to consider that the heat transfer mechanism on the cooling side is not a limiting parameter.

Finally, to compare each geometry, the Nusselt numbers are plotted against the Reynolds number in the results section.

To characterize the global mixing level of each mock-up, the reaction of discolouration of an iodine solution with sodium thiosulfate is implemented according to the following reaction scheme:

$$I_2(\text{brown}) + 2Na_2S_2O_3(\text{colourless}) \rightarrow 2NaI(\text{colourless})$$
$$+ Na_2S_4O_6(\text{colourless})$$

Thiosulfate and iodine concentrations are respectively equal to $1.4 \times 10^{-2}$ mol L⁻¹ and $5 \times 10^{-3}$ mol L⁻¹. The ratio of flowrates is equal to 1 [28].

This homogeneous reaction is instantaneous and mixing limited. As a consequence, at steady state, by measuring the required length to complete the discolouring of iodine, the mixing time can be easily determined. The mixing times are then compared according to both the flow regime and the channel geometry.

Finally, RTD experiments have been carried out in order to characterize the hydrodynamic behaviour in each geometry. A spectro-photometric technique that entails a coloured tracer has been used. Two measuring probes are set up at the inlet and at the outlet of the mock-up. The acquisition time is set to 0.12 s. Each experiment has been performed at room temperature with a flowrate varying from 5 to 18 kg h⁻¹ (Reynolds number range from 450 to 2500). The NETR (Number of Equivalent stirred Tank Reactors) has been assessed from the experimental RTD [29]. The higher NETR is, the more the flow behaves like a plug flow, which is necessary to perform safely and efficiently chemical syntheses.

### 2.4. Numerical simulations

To complete the experimental results and understand the flow mechanisms in the corrugated channel, numerical simulations have been implemented with a commercial CFD code (Fluent). A schematic view of the modelled corrugated channel is illustrated in Fig. 6. The green cross-sections have been defined to visualize the flow all along the straight and the curved lengths.

The numerical results in the cross sections located downstream the 7th bend have been considered to establish the velocity profiles and study the flow mechanisms. The velocity profiles of the Fig. 6 have been plotted versus the radial position upstream the 3rd bend and upstream the 7th one. They perfectly match and thus demonstrate that the flow is established in the portion of interest.

A RNG (Renormalization Group) k-epsilon model has been considered to run the simulations and the mesh size has been optimized to $6 \times 10^5$ cells. Above this value, the numerically measured pressure drops are independent of the mesh size.
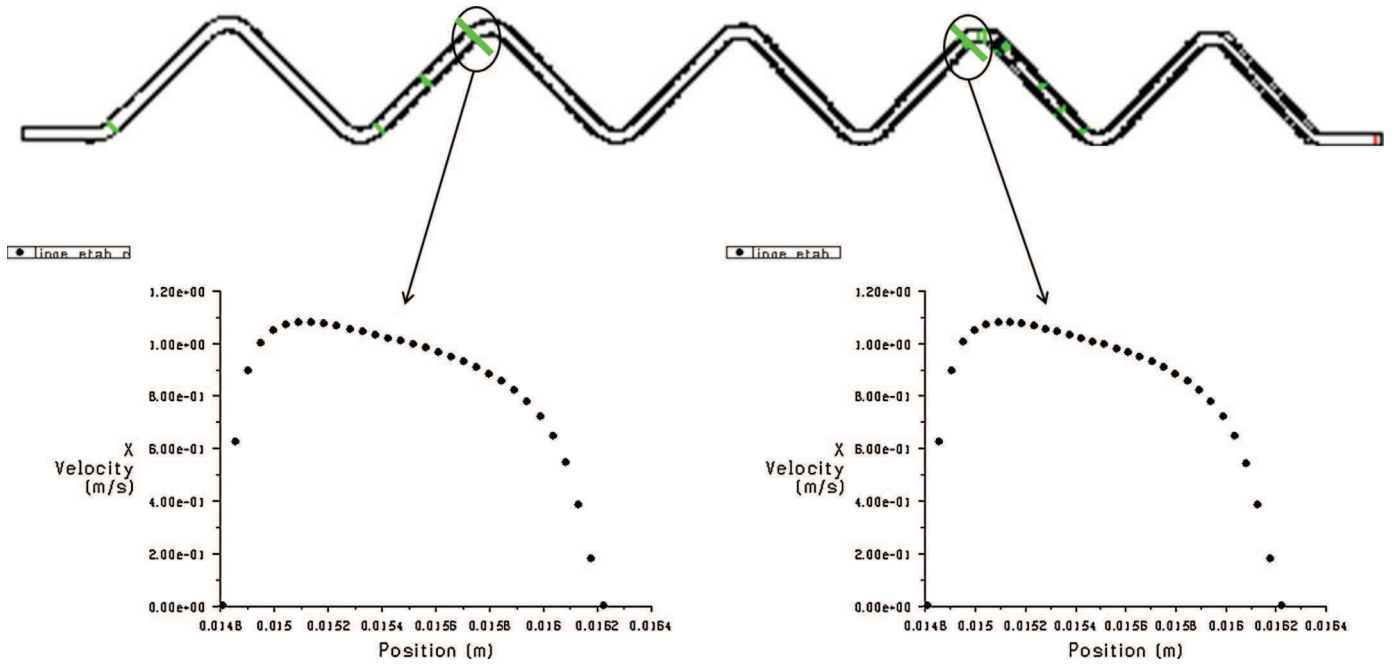
**Fig. 6.** Meshed geometry for the numerical simulations and velocity profiles according to the radial position.

## 3. Results and discussion

The results are divided into two sections. The first one concerns with the influence of the corrugation's geometrical parameters (curvature radius, straight length and bend angle) on both the flow behaviour and the transfer mechanisms. It concerns the mock-ups 'a', 'b', 'c', 'd' and 'e'. The second section is about the first steps towards the scale-up of corrugated channels. The objective is to predict the meandering flow behaviour during the scale-up procedure. Three mock-ups (mock-ups 'e', 'f' and 'g') have been experimentally characterized and compared for that purpose and the influence of the hydraulic diameter and aspect ratio has been investigated.

### 3.1. Influence of the corrugation geometry

#### 3.1.1. Pressure drops

For each geometry (from mock-up 'a' to mock-up 'e'), pressure drops per unit of length versus Reynolds number are plotted in Fig. 7.
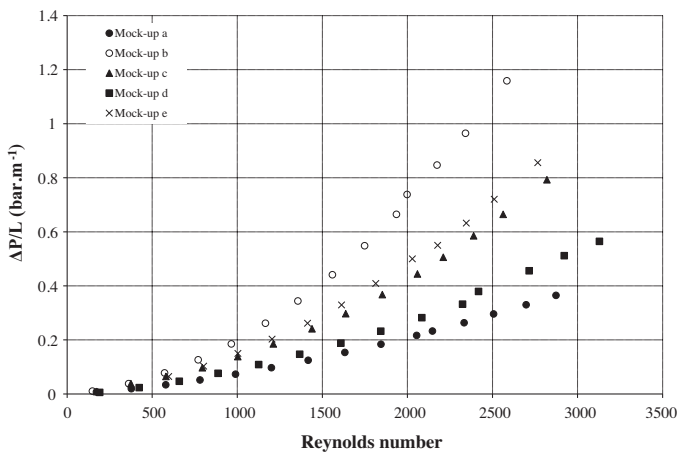
This graph highlights the increase of pressures drops when the number of bends per unit of length increases. Thus, as expected, pressure drops in mock-up 'a' are the lowest ones. This is also the case when geometries 'd' (44 bends/m) and 'c' (106 bends/m) are compared.

If we compare the mock-ups 'b' and 'c', the number of bends per unit of length is very close (90 and 106 bends/m), whereas the bend angle is different (75 and 45°). As a consequence an increase of the bend angle seems to increase the pressure drops.

The increase of the curvature radius also increases the pressure drops. This is the case when mock-ups 'd' and 'e' are compared. The number of bends per unit of length is quite similar (44 and 38 bends/m) whereas the internal curvature radius increases from 0.5 to 3 mm.

The Darcy coefficient, which is characteristic of the size and of the geometry of the channel, has been plotted against the Reynolds number in Fig. 8.

Whatever the geometry, the graph is divided into two zones on both sides of Re = 200. Below this value the Darcy coefficients are
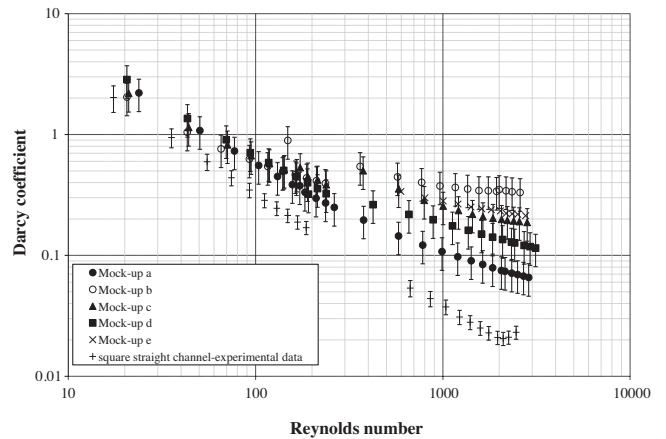


**Fig. 7.** Pressure drop per unit of length versus Reynolds number (water at 25 °C).



**Fig. 8.** Darcy coefficient versus Reynolds number, experiments with water and glycerol (67 w%) at 25 °C.

**Table 2**
Comparison between literature data and numerical results about the pressure drop in a single bend and in a straight length (Re = 686).

| | | Theoretical results (literature correlation) [30] | Numerical results |
|---|---|---|---|
| Bend | Darcy coefficient, $\Lambda$ | 0,27 | – |
| | Pressure drop, $\Delta P$ (P a) | 16,77 | 16,76 |
| Straight length | Darcy coefficient, $\Lambda$ | 0,084 | – |
| | Pressure drop, $\Delta P$ (P a) | 16,82 | 45,53 |

close to the characteristic value of a straight channel. In this regime (viscous fluids applications for instance), the effect of the bends on the pressure drops is quite negligible. The transition begins around Re = 200. This may be linked to the formation of Dean vortices around De = 150 [16]. This critical value corresponds to a Reynolds number of 130 in mock-ups 'b', 'c' and 'd' and 212 in mock-up 'e'. Above Re = 200 and as already observed in Fig. 7, the main parameters are the corrugation angle (mock-up 'b' vs. mock-up 'c'), the number of bends per unit of length (mock-up 'c' vs. mock-up 'd') and the curvature radius (mock-up 'd' vs. mock-up 'e'). These three parameters are actually responsible for the increase of the curved length/straight length ratio which promotes pressure drops.

For each mock-up, the straight length is given in Table 1 whereas the curved length for one bend is assessed from the following equation:

$$L_{curved} = \theta \times R_c$$

From the previous experimental results, the pressure drop of one bend has been deduced for each geometry. It includes the pressure drop due to the curved length itself and the one due to the propagation of the bend vortices along the downstream straight length. The simulation results highlight these two pressure drop components in Table 2.

The pressure drop assessed in a bend is exactly the same given by literature correlation or simulation results (16.77 Pa). The upstream corrugations have actually no influence on the considered bend in these simulation flow conditions. The flow is laminar at the bend inlet. The pressure drop in the straight length has been theoretically assessed considering no upstream bend ($\Lambda = 0.9 \times 64/Re$). It is 3 times lower than in the simulated straight length downstream the bend. This highlights the pressure drop component due to the vortices propagation. Fig. 9 illustrates this phenomenon.

The highest intensity of the counter-rotating vortices is observed at the bend outlet (S1 on Fig. 9). Then the intensity decreases all along the channel length before disappearing at S4. S5 shows that the flow became laminar again with the axial velocity peak slightly off-centred because of the bend centrifugal force.

The following graph (Fig. 10) shows the pressure drop per bend for each geometry. It has been assessed by removing the theoretical pressure drop due to the straight lengths from the global pressure drop. Then, this remaining pressure drop has been divided by the number of bends. As a consequence, the pressure drop per bend takes into account the pressure drop due to both the curved length of the bend and the vortices propagation.

The pressure drop per bend is higher in the mock-up 'd' than in the mock-up 'c' whereas the opposite trend was observed in Figs 7 and 8. Since the geometrical parameters of the bends ($R_c$ and $\theta$) are the same, the curved length generates the same pressure drop. The difference comes actually from the straight length along which the vortices are propagated. This length is indeed three times higher in the mock-up 'd' than in the mock-up 'c' (20.28 mm vs. 6.94 mm). Thus, the pressure drop due to the propagation of the bend vortices increases the pressure drop per bend of mock-up 'd'.
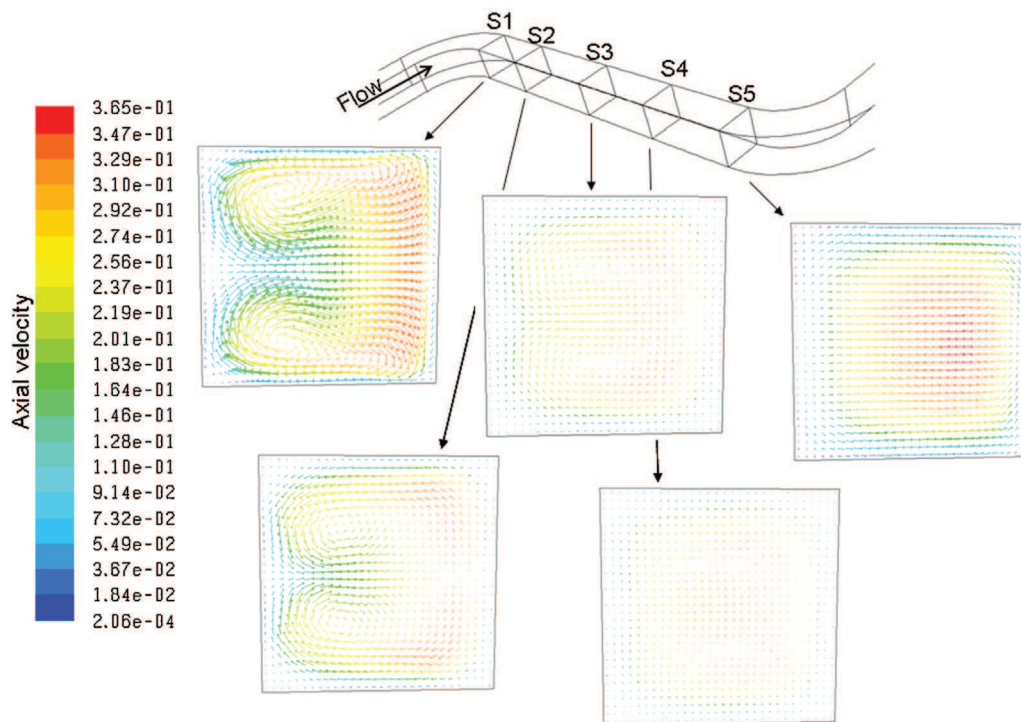


**Fig. 9.** Velocity profiles in cross section of the corrugated channel (mock-up 'e').
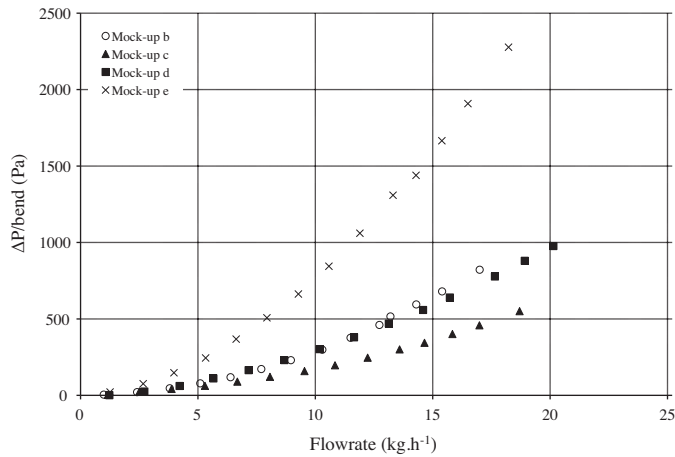
**Fig. 10.** Influence of the geometry and the flowrate on the pressure drop of one bend (curved length + vortices propagation).



**Fig. 11.** Number of equivalent stirred tank reactor (NETR) per unit of length vs. Reynolds number for each mock-up geometry.

In the mock-up 'b', the straight length is equal to 6.94 mm but the corrugation angle is higher than in the mock-up 'c' (respectively 75° and 45°), the bend pressure drop is thus higher.

Finally, the highest pressure drop per bend is observed in mock-up 'e'. This is due to the curved length which is actually 2.6 times longer than the one of mock-up 'd' with the same straight length. This is the influence of the internal curvature radius.

Finally, it can be established that pressure drops in a corrugated channel are made of three components: the pressure drop in the straight lengths, the pressure drop in the curved lengths and the pressure drop due to the propagation of the vortices downstream each bend.

The straight length between two bends seems to be the key parameter. Its increase reduces the number of bends per unit of length and thus the total pressure drop. However, when the straight length is lower than the propagation length, its increase promotes the propagation of the vortices and thus the pressure drop. This increases the pressure drop per bend until reaching a maximal value when the straight length is equal to the propagation one.

The pressure drop also depends on the corrugation angle. The higher the corrugation angle, the higher the curved length, thus promoting the pressure drops (see Eq. (6)).

Finally, the pressure drop profiles are strongly dependent on the number of bends and on their geometry. The following section details their influence on the RTD.

### 3.1.2. Residence time distribution

The RTD has been investigated for each geometry (mock-ups 'a' to 'e'). The following graph (Fig. 11) illustrates the experimental results. The number of equivalent stirred tank reactors (NETR) per unit of length has been assessed in each mock-up.

First of all, whatever the geometry, the NETR is high enough (NETR > 50 for mock-ups from 3.4 to 5 m long) to consider that the flow behaves like a quasi-plug flow. However the influence of the wavy geometry on NETR is not negligible. As highlighted in the pressure drop study, the main parameters are also the number of bend per unit of length and the ratio between the curved length and the straight one. On Fig. 11, the NETR of mock-up 'c' is around 2 times higher than the NETR of mock-up 'd'. The bends of these geometries are strictly the same (curvature radius and corrugation angle). Thus, the difference lies on the straight length between two bends and as a consequence on the number of bends per unit of length which promotes the plug flow behaviour. Actually, the flow instabilities generated in each bend promote the radial
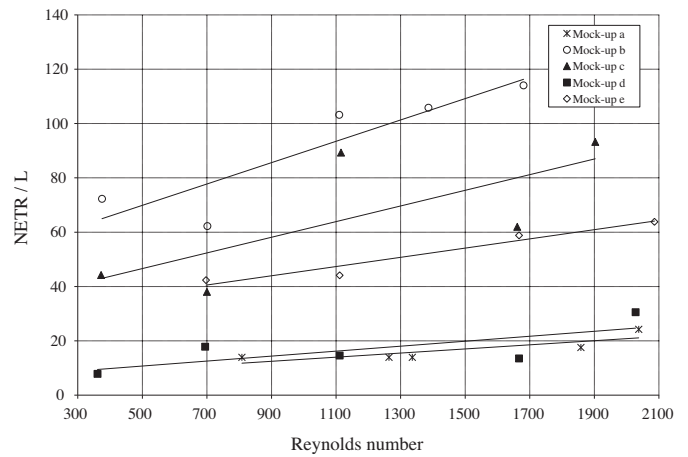
homogenization of the concentration gradients which reduces axial dispersion.

Similarly, the increase of the ratio between the curved length and the straight one, leads to an increase of the NETR per unit of length. The NETR per unit of length in mock-up 'b' and mock-up 'e' are respectively higher than in mock-up 'c' and mock-up 'd'. This is due to their ratio between the curved length and the straight one which increases with the increase of the bend angle (mock-up 'b' compared to mock-up 'c') or the curvature radius (mock-up 'e' compared to mock-up 'd'), the other geometrical parameters being kept constant.

These results are confirmed with the graph of Fig. 12 which shows the influence of the wavy geometry on the NETR per bend.

On Fig. 12, the NETR in the mock-ups 'c' and 'd' are very close. The bends are strictly identical and so is their influence on the RTD measurements. Thus this is, indeed, the bends which govern the RTD and the higher the number of bends per unit of length, the narrower the RTD.

The decrease of the NETR/bend between mock-ups 'b' and 'c' or between mock-ups 'e' and 'd' may be due to two effects. The first one is the decrease of the ratio between curved length and straight length. The second one could be due to the appearance of axial re-circulating cells generated downstream each bend when the curvature radius decreases [26,31]. This phenomenon creates recirculating zones downstream each bend that could disturb the plug flow behaviour.
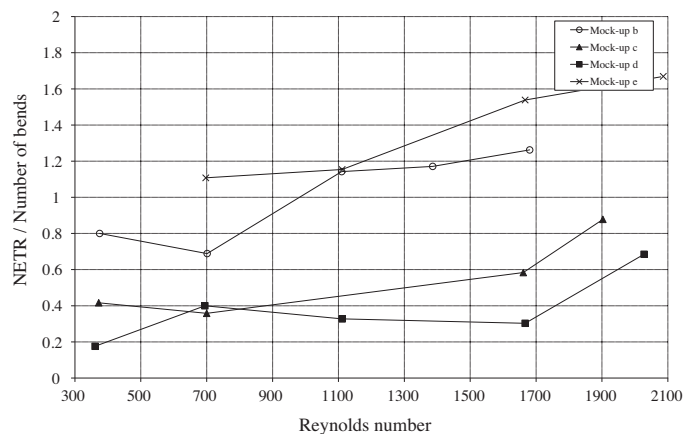


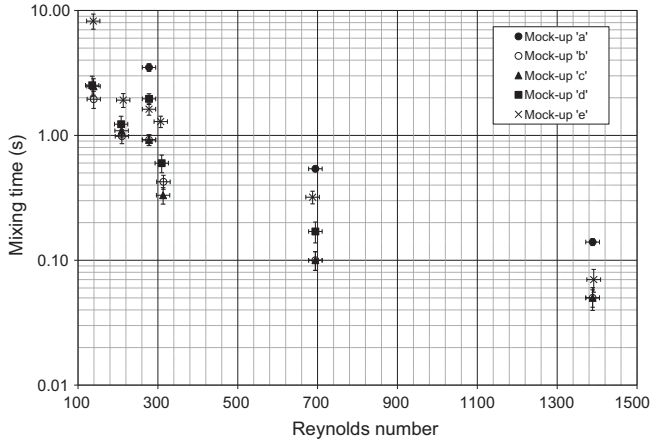**Fig. 12.** Influence of the Reynolds number and the geometry on the RTD.

**Fig. 13.** Mixing times vs. Reynolds number according to the corrugation geometry.



**Fig. 14.** Mixing times vs. Dean number according to the corrugation geometry.

However, whatever the geometry, the number of bends per unit of length and the NETR per bend are high enough to assume a quasi plug flow whatever the channel design.

### 3.1.3. Mixing performances

Mixing performances have been assessed by measuring the mixing times versus the Reynolds number. Results are given in Fig. 13. As expected, the trend is as follows: the mixing times are decreasing with the increasing Reynolds number.

Whatever the Reynolds number, mixing times in the mock-up 'a', which is made of 90 mm straight lengths and 180° turning bends, are higher than in the corrugated geometries (mock-ups 'b' to 'e'). Moreover, the influence of the geometry is relevant for lower Reynolds number. Above Re = 700, mixing times tend to be similar whatever the corrugation (except for mock-up 'a').

At a constant Reynolds number, mixing in mock-up 'e' is less efficient than in the other corrugated mock-ups with a gap around Re = 150. This result may be due to the flow structure which is different in the mock-up 'e'.

In the literature, the critical Dean number, above which the Dean vortices appear, is estimated between 100 and 250 [16]. These vortices promote the homogenization of the temperature, the velocity but also the concentration gradients. Thus it contributes to improve the mixing performances of the corrugated flow.

In our experiments, the geometrical parameter which is different between mock-up 'd' and mock-up 'e' is the curvature radius (respectively 1.5 and 4 mm). As a consequence, when the Reynolds number equals 150, the Dean number equals 160 in the mock-up 'd' and 100 in the mock-up 'e'. Thus it seems that the critical Dean number has been reached in mock-up 'd' (and also in mock-ups 'b' and 'c') which is not the case for mock-up 'e'. The Fig. 14 illustrates this result by considering the mixing times versus the Dean number.

These results confirm the former hypothesis since for a constant Dean number the mixing performances are equal whatever the geometry. The curvature radius will be thus an important parameter to be considered for mixing applications and particularly with viscous fluids for which the Reynolds numbers are low.

### 3.1.4. Thermal performances

From temperature measurements, the influence of wavy geometries on the thermal performances is studied. In that way, an intensification factor is introduced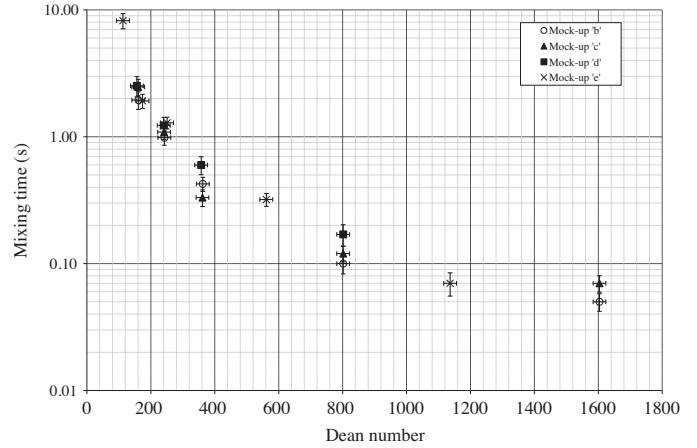. It takes into account the global heat transfer coefficient, $U$ (W m$^{-2}$ K$^{-1}$) but also the geometry compactness. It is defined as:

$$\frac{U \times A}{V}(\text{Wm}^{-3}\text{K}^{-1})$$

with $A$ the heat exchange area (m$^2$) and $V$ the volume of fluid (m$^3$). The graph of Fig. 15 shows the intensification factor versus the flow rate for each geometry.

First, as obtained during the pressure drop and the RTD studies, the influence of the number of bends per unit of length is relevant. The intensification factor almost reaches a ratio of 2 between geometry 'c' (106 bends/m) and 'd' (44 bends/m).

Unlike RTD and pressure drop measurements, the influence of the corrugation angle seems here to be negligible since the curves of geometries 'c' ($\theta$ = 45°) and 'b' ($\theta$ = 75°) are superposed. Finally, an increase of the curvature radius from 1.5 (geometry 'd') to 4 mm (geometry 'e') leads to a decrease of the intensification factor. Two effects are involved; the decrease of the number of bends per unit of length (from 44 to 38 bends/m) and the decrease of the Dean number (for a constant flow rate) which leads to a decrease of re-circulating cells intensity. This phenomenon is illustrated in Fig. 16.

The effects of both the number of bends per unit of length (mock-up 'c' vs. mock-up 'd') and the corrugation angle (mock-up 'b' vs. mock-up 'c') are obviously unchanged. However, as observed for mixing characterizations, the Dean number is still the relevant dimensionless number when the curvature radius is considered. Indeed, similar profiles are obtained for both geometries 'd' ($R_c$ = 1.5 mm) and 'e' ($R_c$ = 4 mm).
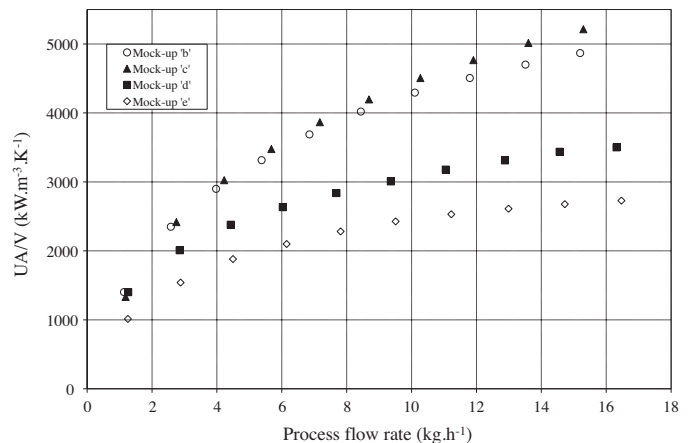


**Fig. 15.** Intensification factor vs. flow rate according to the wavy geometry.
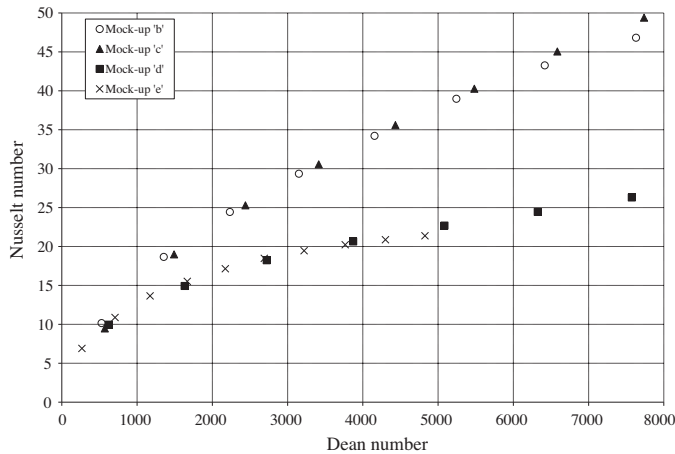
**Fig. 16.** Nusselt number vs. Dean number according to the corrugation geometries.

The results of the thermal characterizations complete the previous experimental results. The Dean number seems to be the relevant parameter and then the influent geometrical parameter is the number of bends per unit of length.

### 3.1.5. Conclusion of the parametric study

The influence of the geometrical parameters of a wavy channel on heat transfer, pressure drops, mixing performances and residence time distribution has been investigated in the first part of this work. The main goal was to study and to understand both the thermo-hydraulic mechanisms and the flow behaviour in the corrugated channel of a plate heat exchanger/reactor. The trends are obviously different and the most efficient geometry will depend on the chosen performance criteria. Actually, the most efficient mock-ups in terms of heat and mass transfers and/or momentum often generate many flow instabilities. As a consequence performance criteria have to be compared to each other to find the optimal geometry. It will depend on both the end-using specifications and the aimed versatility of the heat exchanger/reactor. For instance, it is interesting to plot the thermal performances vs the pumping power as illustrated on Fig. 17.

This graph shows that for a fixed pumping power, the mock-up 'c' is the most efficient concerning the heat transfer criterion. The mock-up 'b' generates too high pressure drops for an equivalent intensification factor (see Fig. 15).

Moreover, although pressure drops decrease between the mock-ups 'c' and 'd' (because of the decrease of the bend number per
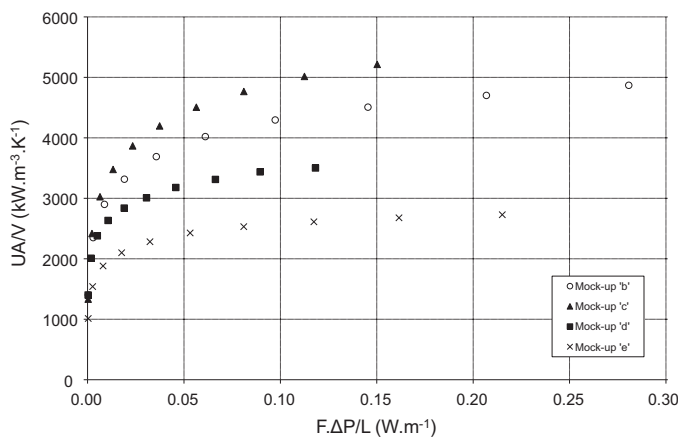


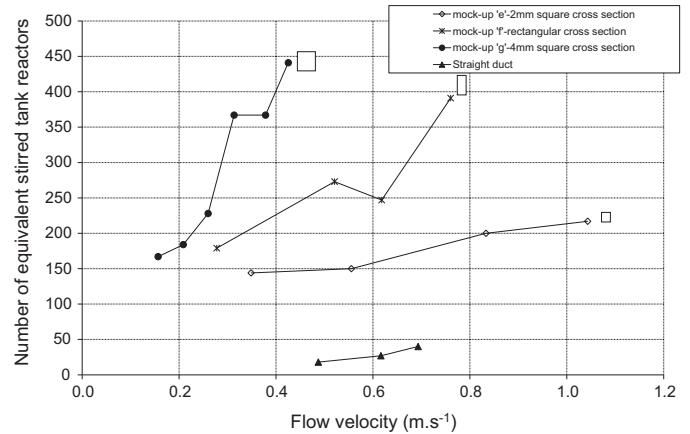**Fig. 17.** Intensification factor vs. pumping power per unit of corrugated channel length.

unit of length from 106 to 44 bends/m), it does not balance the decrease of heat transfer coefficient. So as illustrated in Fig. 17, the mock-up 'd' is less efficient than the mock-up 'c' if we consider the intensification factor vs. the pumping power.

However, many other criteria, like compactness, manufacturing costs,... can be considered. In that case, the ranking of the corrugated geometries may change.

The first part of this work shows that the influence of each geometrical parameter depends on the considered performance criterion. That is the reason why an optimization regarding the specifications and the technology use is required. Once the optimum geometry is defined and to expect a future industrialization, the performance prediction during the scale-up procedure is required. The first steps towards the scale-up of corrugated channel are described in the following part of this paper.

### 3.2. Influence of both the hydraulic diameter and the aspect ratio

Three mock-ups ('e', 'f' and 'g') are considered in this section. The channels of mock-ups 'e' and 'g' are respectively 2 mm and 4 mm square-cross section. The mock-up 'f' is made of a rectangular cross section channel of 2 mm large and 4 mm in-depth.

#### 3.2.1. Residence time distribution

The RTD has been experimentally investigated for those three geometries. The following graph illustrates the number of equivalent stirred tank reactors (NETR) versus the flow velocity in each geometry. The RTD measurements have also been implemented in a rectangular cross-section ($2 \times 4$ mm$^2$) straight channel.

For each corrugated geometry, the NETR is high enough (NETR > 150) to consider that the flow behaves like a plug flow in the corrugated channels whatever the characteristic size. This is not true in the rectangular cross section straight duct, since the NETR is less than 50.

During the scale-up procedure, the residence time has to be kept constant to complete the chemistry. Since the developed length of the three mock-ups is the same, the comparison at a constant flow velocity is of interest. The graph of Fig. 18 shows that the higher the hydraulic diameter, the narrower the RTD. This is actually the Reynolds number influence which increases with the hydraulic diameter. Thus, if the flow velocity is equal to 0.3 m s$^{-1}$, the Reynolds number is respectively of 600, 800 and 1200 in the mock-ups 'e', 'f' and 'g'. The following graph represents the NETR versus the Reynolds number.

The comparison between Figs. 18 and 19 highlights the interest of considering the Reynolds number during the scale-up process. However there is still a difference between each geometry,
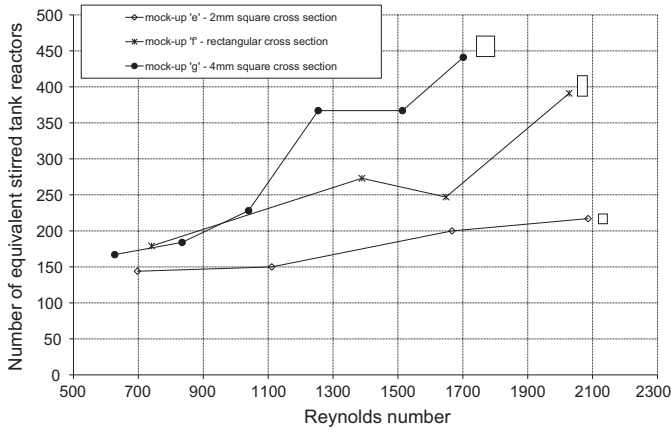


**Fig. 18.** Influence of the flow velocity and the channel size on the RTD.
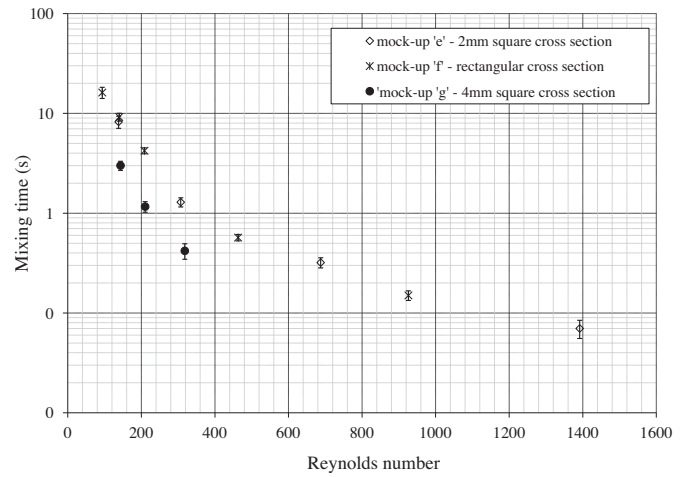
**Fig. 19.** NETR vs. Reynolds number.



**Fig. 21.** Mixing times vs. Reynolds number according to the channel design.

especially above Re = 1000. This could be due to the internal Dean number influence which tends to increase with the increase of the channel size (because of both the increase of the hydraulic diameter and the decrease of the internal curvature radius). Therefore, the NETR is plotted versus the Dean number in the following graph (Fig. 20).

The characteristic curves are very close each other, highlighting the relevance of considering the internal Dean number. Actually, the scale-up process does not penalize the plug flow characteristics which are even improved if the flow velocity or the Reynolds number are kept constant. The performances are maintained with the internal Dean number which is an interesting result to predict the flow behaviour during the scale-up step.

### 3.2.2. Mixing performances

The mixing performances have been assessed by measuring the mixing times versus the Reynolds number. The results are given in Fig. 21.

The mixing times are quickly decreasing with the increase of the Reynolds number. The mock-up 'g' is more effective in terms of mass transfer than the other ones, this could be due to the Dean number as observed during the RTD experiments. On the other hand, the mixing times of mock-ups 'e' and 'f' are quite close. The internal curvature radiuses of these two geometries are actually similar (3 mm). As a consequence when the Reynolds number is

equal, the ratio between the Dean numbers of both mock-ups 'e' and 'f' is equal to:

$$\frac{De_{'e'}}{De_{'f'}} = \frac{Re_{'e'}}{Re_{'f'}} \times \sqrt{\frac{d_{h_{'e'}}}{d_{h_{'f'}}}} = 1 \times \sqrt{\frac{2}{2.67}} = 0.9 \tag{11}$$

This ratio is close to 1 and that could be the reason why the characteristic curves are very close. On the other hand, the Dean number ratio between mock-ups 'e' and 'g' is equal to:

$$\frac{De_{'e'}}{De_{'g'}} = \frac{Re_{'e'}}{Re_{'g'}} \times \sqrt{\frac{d_{h_{'e'}}/R_{c_{'e'}}}{d_{h_{'g'}}/R_{c_{'g'}}}} = 1 \times \sqrt{\frac{2/3}{4/2}} = 0.6 \tag{12}$$

Dean numbers in mock-ups 'e' and 'g' are quite different and the flow might not have the same behaviour. This is what is observed when plotting the mixing times versus the Dean number in Fig. 22.

As observed during the RTD experiments, the Dean number is still the relevant parameter to predict the performances during the scale-up procedure from 2 to 4 mm. However, whatever the considered scale-up parameter (velocity, Reynolds number or Dean number), the mixing performances do not decrease during the scale-up process and are even improved. As a conclusion, both RTD and mass transfer are not limiting processes during the scale-up here from 2 to 4 mm.
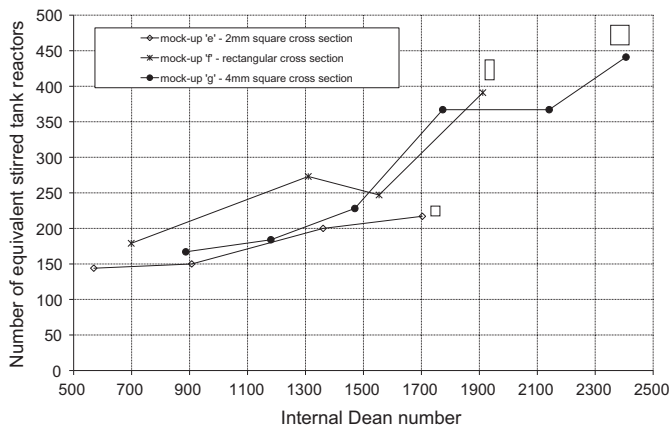


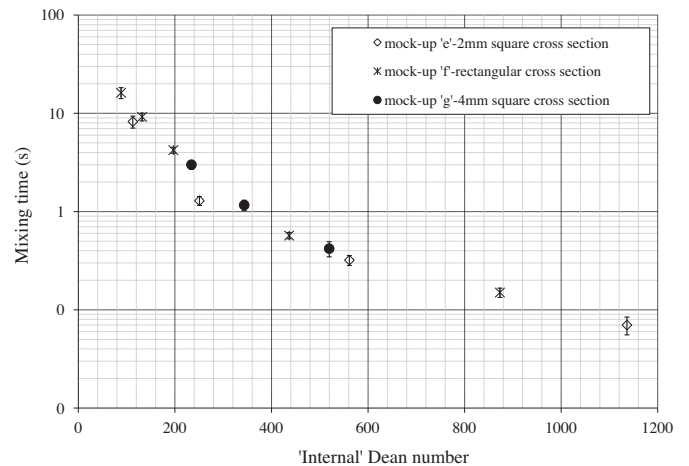**Fig. 20.** NETR vs. internal Dean number.



**Fig. 22.** Mixing times vs. Dean number according to the channel characteristic size.
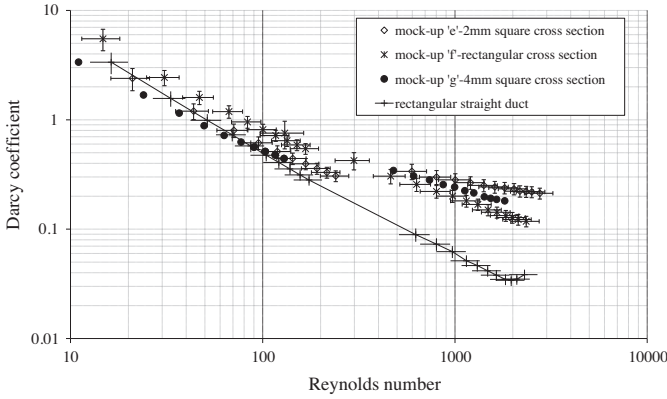
**Fig. 23.** Darcy coefficient vs Reynolds number, experiments with water and glycerol (67 w%) at 25 °C.

### 3.2.3. Pressure drops

The Darcy coefficient, which is characteristic of the size and of the geometry of the channel, has been plotted against the Reynolds number in Fig. 23.

Whatever the geometry, the graph is divided into two zones apart Re = 200. Below this value the Darcy coefficients are close to the value typical of a straight channel. In this regime (viscous fluids applications for instance), the effect of the bends on the pressure drops is quite negligible. However, it can be noticed that the Darcy coefficients of the two square cross section mock-ups are each other closer than with the rectangular cross section mock-up. As a consequence, when the aspect ratio is kept constant, the Darcy coefficient can be correlated to the Reynolds number in the very laminar regime (Re < 200):

$$\Lambda = 21.3 \cdot Re^{-0.78} \tag{13}$$

Both the rectangular corrugated channel and the rectangular straight one lead to higher pressure drops in the low Reynolds regime (Re < 200). Since the corrugations have few effects on the pressure drop, the difference between square and rectangular cross sections may be due to the aspect ratio effect which has been studied by Shah & London [32] and is illustrated in Fig. 24.

Shah & London [32] showed that the friction factor increases when the aspect ratio decreases. This is what is observed in Fig. 23 below Re = 200. Beyond Re = 200, the channel characteristic size begins to influence the Darcy coefficients. This may be the Dean number influence as illustrated on the graph of Fig. 25.

Considering the square cross section corrugated channels, the Darcy coefficient curves of both geometries 'e' and 'g' are very close each other above Re = 200. In this regime the Dean number is again the relevant dimensionless number governing the flow. It allows the prediction of pressure drops during the scale-up procedure and the following correlation can be used for corrugated millichannels:

$$\Lambda = 3.68 \times De_i^{-0.38} \tag{14}$$

The influence of the aspect ratio is significant whatever the flow regime. Below Re = 200, the rectangular cross section tends to promote the Darcy coefficient whereas beyond Re = 200 the Darcy coefficient in the rectangular cross section channel is lower than in the square cross section channel. The influence of this parameter should be further studied.

### 3.2.4. Thermal performances

The graph on Fig. 26 plots the Nusselt number versus the Reynolds number obtained in each corrugated geometry.

This graph highlights two results. The first one is the improvement of the thermal performances with the increase of the
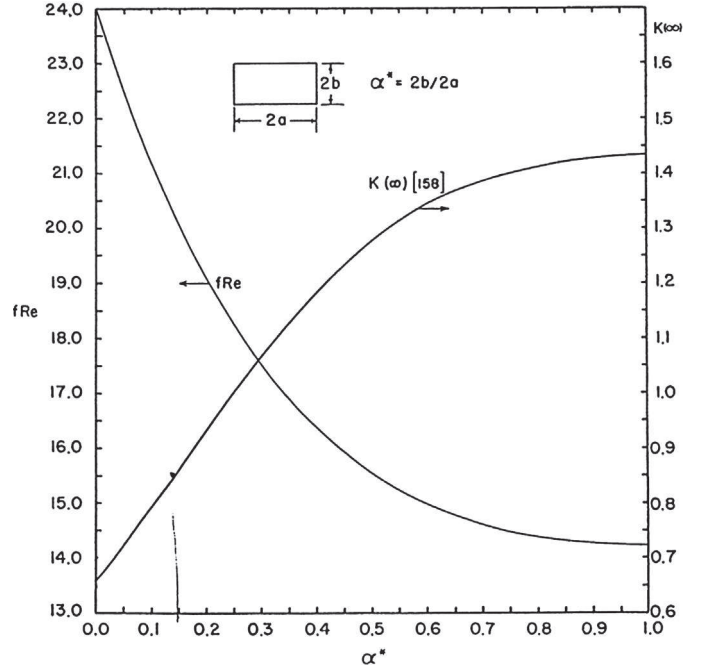


**Fig. 24.** Friction factor (equivalent to the Darcy coefficient) vs aspect ratio in a laminar regime [31].

hydraulic diameter (from 2 to 4 mm). This may be due to the Dean number influence. The second result is the influence of the aspect ratio. The cross section elongation from 1 to 0.5 seems to improve the thermal performances. This is not the tendency observed by Shah & London [32] in a straight rectangular duct (case 4 on Fig. 27).

However, unlike Shah & London [32], the present work concerns corrugated channel and the aspect ratio seems to have an influence on the radial recirculation loops. Indeed, in a rectangular cross section channel, in addition to the counter rotating vortices close to the wall, additional vortices appear in the cross section along the outer wall (Fellouah et al., [16]). This is illustrated in the Fig. 28 where velocity profiles have been plotted upstream a bend in mock-ups 'e', 'f' and 'g' (Re = 400).

Given a Reynolds number, the additional vortices observed in the rectangular cross section promote the homogenization of temperature gradient. The better heat performances observed in the mock-up 'f' may be due to this phenomenon. However further developments are required, particularly to dissociate the aspect
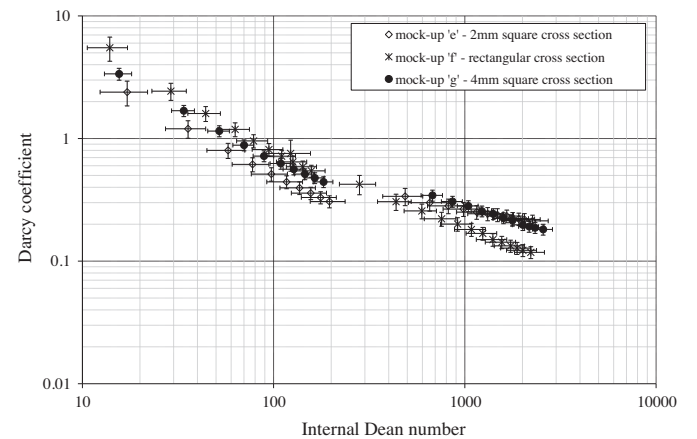


**Fig. 25.** Darcy coefficient vs. Dean number, experiments with water and glycerol (67 w%) at 25 °C.
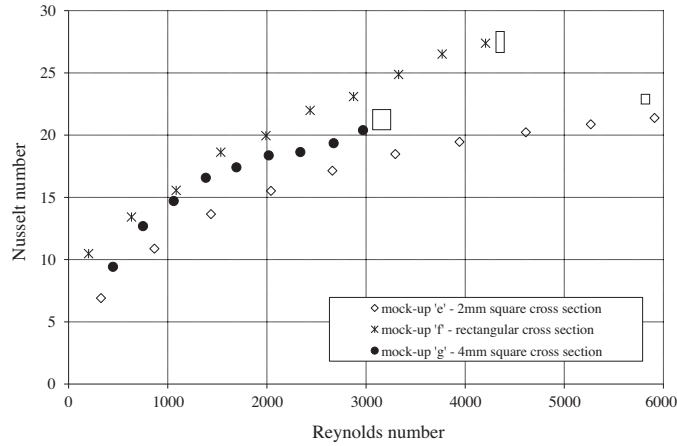
**Fig. 26.** Nusselt number vs Reynolds number according to the corrugation geometries.
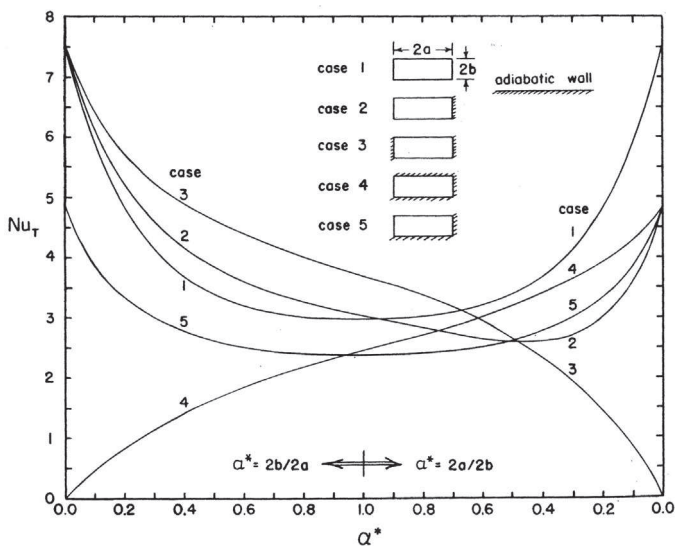


**Fig. 27.** Nusselt number (constant wall temperature) vs aspect ratio in a laminar regime and straight duct. Mock-up 'f' configuration is compared with case 4 with $\alpha^* = 2b/2a = 0.5$ (Shah & London, 1978).

ratio influence from the one of the ratio between curvature radius and hydraulic diameter. These both parameters are indeed varying in the mock-up 'f' compared to mock-ups 'e' and 'g'.

The Nusselt number vs the Dean number has been plotted for the two square cross section geometries (see Fig. 29).

Given a constant Dean number the heat transfer performances are very close whatever the channel hydraulic diameter. Unlike straight tube correlations of Nusselt number vs Reynolds number, the heat transfer performances of a corrugated channel seem to depend on the Dean number. This noticeable result shows that as long as the Dean number is kept constant, the scale-up procedure (here from 2 to 4 mm hydraulic diameter) has no effect on the Nusselt number.

As a consequence a Nusselt number correlation has been established:

$$Nu = 0.45 \times De_i^{0.43} \times Pr^{0.33} \qquad (15)$$

This correlation is the first brick for the prediction of heat transfer performances during the scale-up process of corrugated milli-channels.
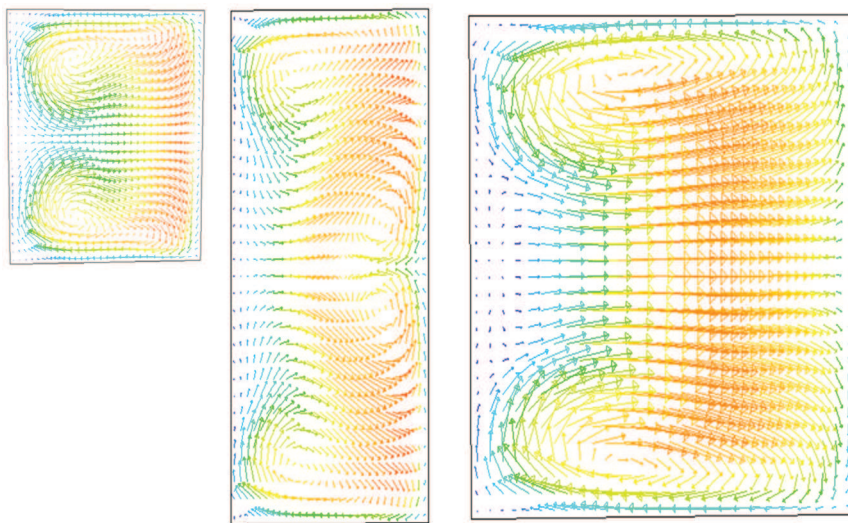


**Fig. 28.** Velocity profiles at the bend outlet in mock-ups 'e', 'f' and 'g' (Re = 400).
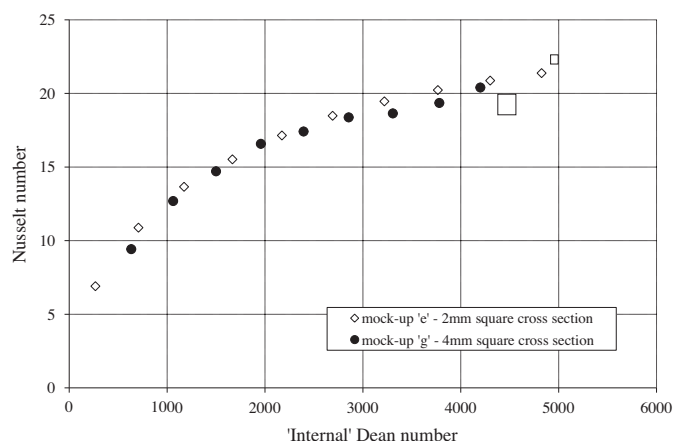
**Fig. 29.** Nusselt number vs. internal Dean number for the square cross section mock-ups.

## 4. Conclusion and perspectives

The influence of the geometrical parameters and characteristic size of a wavy channel on heat transfer, pressure drops, mixing performances and residence time distribution have been investigated in this work. The main goal was to study and to understand both the thermo-hydraulic mechanisms and the flow behaviour in the corrugated channel of a plate heat exchanger/reactor. This is the first step of the geometry optimization and the component scale-up. Then the second objective was to establish correlations to predict the flow behaviour during the channel scale-up procedure.

The RTD characterizations, modelled by N-tank in series, showed that whatever the geometry and the flow regime ($200 \leq Re \leq 2100$), the flow behaves like a quasi-plug flow and the number of bends is the relevant parameter. As a consequence it can be limited to a minimum value. This result is interesting facing the pressure drops since the lower the number of bends, the lower the pressure drop. Three pressure drop components have been identified: the one due to the straight length, the one due to the curved length and the pressure drop due to the propagation of the vortices generated in the bend. Actually, the longer the straight length, the higher the pressure drop per bend (because of vortices propagation) but the lower the total pressure drop (due to number of bend per unit of length). Moreover, the pressure drop increases when the ratio between straight length and curved length decreases, i.e. when the corrugation angle or the curvature radius increase.

The second part of the experimental characterization concerns the heat and mass transfer assessments. The mixing times are homogeneous whatever the geometry above Re = 700. Under this value, the mixing times mainly depend on the curvature radius. The relevant dimensionless number is no longer the Reynolds number but actually the Dean number which takes into account the vortices generated in each bend. The heat transfer performances are more sensitive to the channel geometry. They depend on the number of bends per unit of length and of the curvature radius. The Dean number is again the relevant dimensionless number. The Nusselt number curves vs. Dean number are similar whatever the curvature radius is.

In order to avoid complex heat exchanger/reactor geometries which could generate high manufacturing and operating costs, the idea was to study a simple 2D process channel geometry. This work led to a better understanding of the flow mechanisms in the corrugated channel. The main objective is then to optimize the channel geometry depending on the process constraints. The second step of this work was to derive design rules and correlations to scale-up these apparatuses from lab-scale to pilot-scale.

The effects of the hydraulic diameter and the aspect ratio of wavy channels on heat transfer, pressure drops, mixing and residence time distribution have been investigated in that purpose. The main goal was to study the evolution of these performance criteria during the scale-up process.

When increasing the channel characteristic size, RTD results and mass transfer are improved with respectively narrower RTD and shorter mixing times. However the main result concerns the relevance of the internal Dean number to predict the corrugated flow behaviour. This dimensionless number is assessed from the internal curvature radius. Thus for a given Reynolds number, the hydraulic diameter increase, which induces a curvature radius decrease, has strong effect on the Dean number. Nusselt numbers and Darcy coefficients are also directly linked to the internal Dean number and remain constant during the scale-up process from 2 to 4 mm providing that the aspect ratio is equal to 1.

The established correlations are the first step towards the flow behaviour prediction during the scale-up process. However it would be interesting now to dissociate the effect of the aspect ratio from the hydraulic diameter one with additional mock-ups and to transpose these correlations to a $100\,L\,h^{-1}$ pilot in order to assess their relevance.

## References

[1] A. Stankiewicz, J.A. Moulijn, Process intensification: transforming chemical engineering, Chem. Eng. Prog. 96 (2000) 22–34.

[2] Z. Anxionnaz, M. Cabassud, C. Gourdon, P. Tochon, Heat exchanger/reactors (HEX Reactors): concepts, technologies: state-of-the-art, Chem. Eng. Process. 47 (2008) 2029–2050.

[3] Z. Anxionnaz, M. Cabassud, C. Gourdon, P. Tochon, Transposition of an exothermic reaction from a batch reactor to an intensified one, Heat Transfer Eng. 31 (2010) 788–797.

[4] R.K. Shah, A.C. Mueller, Heat exchange in Ullmann's encyclopaedia of industrial chemistry, unit operations II, vol B3, ed., Wiley-VCH, Weinheim, Germany, 2002, pp. 11–15.

[5] B. Thonon, P. Tochon, Compact multifunctional heat exchangers: a pathway to process intensification, in: A. Stankiewicz, J. Moulijn (Eds.), Re-engineering the chemical processing plant, Marcel dekker, New York, 2004, pp. 121–127.

[6] S. Ferrouillat, P. Tochon, H. Peerhossaini, Micromixing enhancement by turbulence: application to multifunctional heat exchangers, Chem. Eng. Process. 45 (2006) 633–640.

[7] L. Prat, A. Devatine, P. Cognet, M. Cabassud, C. Gourdon, S. Elgue, F. Chopard, Performance evaluation of a novel concept « open plate reactor » applied to highly exothermic reactions, Chem. Eng. Tech. 28 (2005) 1028–1034.

[8] P. Tochon, R. Couturier, Z. Anxionnaz, S. Lomel, H. Runser, F. Picard, A. Colin, C. Gourdon, M. Cabassud, H. Peerhossaini, D. Della Valle, T. Lemenand, Toward a competitive process intensification: a new generation of heat exchanger-reactors, Oil Gas Sci. Technol. 65 (2010) 785–792.

[9] C. Habchi, T. Lemenand, D. Della Valle, H. Peerhossaini, Turbulent mixing and residence time distribution in novel multifunctional heat exchangers-reactors, Chem. Eng. Process. 49 (2010) 1066–1075.

[10] C. Habchi, D. Della Valle, T. Lemenand, Z. Anxionnaz, P. Tochon, M. Cabassud, C. Gourdon, H. Peerhossaini, A new adaptive procedure for using chemical probes to characterize mixing, Chem. Eng. Sci. 66 (2011) 3540–3550.

[11] L. Despenes, S. Elgue, C. Gourdon, M. Cabassud, Impact of the material on the thermal behaviour of HEX reactors, Chem. Eng. Process. 52 (2012) 102–111.

[12] M. Roudet, K. Loubiere, C. Gourdon, M. Cabassud, Hydrodynamic and mass transfer in inertial gas-liquid flow regimes through straight and meandering millimetric square channels, Chem. Eng. Sci. 66 (2011) 2974–2990.

[13] F. Theron, Z. Anxionnaz-Minvielle, N. Le Sauze, M. Cabassud, Transposition from a batch to a continuous process for microencapsulation by interfacial polycondensation, Chem. Eng. Process. 54 (2012) 42–54.

[14] Z. Anxionnaz, F. Theron, P. Tochon, R. Couturier, P. Bucci, F. Vidotto, C. Gourdon, M. Cabassud, S. Lomel, G. Bergin, S. Bouti, H. Peerhossaini, T. Lemenand, C. Habchi, RAPIC project: toward competitive heat-exchanger/reactors, in: The 3rd European Process Intensification Conference (EPIC), June 20–23, Manchester, UK, 2011.

[15] W.R. Dean, Fluid motion in a curved channel, P. R. Soc. London Series A 121 (1928) 402–420.

[16] H. Fellouah, C. Castelain, A. Ould El Moctar, H. Peerhossaini, A criterion for detection of the onset of Dean instability in Newtonian fluids, Eur. J. Mech. B-Fluids 25 (2006) 505–531.

[17] S. Sugiyama, T. Hayashi, K. Yamazaki, Flow characteristics in the curved rectangular channels, B. Jpn Soc. Mech. Eng. 26 (1983) 964–969.

[18] F. Jiang, K.S. Drese, S. Hardt, M. Küpper, F. Schönfeld, Helical flows and chaotic mixing in curved micro channels, AIChE J. 50 (2004) 2297–2305.

[19] N.R. Rosaguti, D.F. Fletcher, B.S. Haynes, Laminar flow and heat transfer in a periodic serpentine channel, Chem. Eng. Technol. 28 (2005) 353–361.

[20] K.C. Cheng, J. Nakayama, M. Akiyama, Flow Visualisation International Symposium, Tokyo, 1977, pp. 181.

[21] P.M. Ligrani, S. Choi, A.R. Schallert, P. Skogerboe, Effects of Dean vortex pairs on surface heat transfer in curved channel flow, Int. J. Heat Mass Tran. 39 (1996) 27–37.

[22] T.T. Chandratilleke, A. Nursubyakto, Numerical prediction of secondary flow and convective heat transfer in externally heated curved rectangular ducts, Int. J. Therm. Sci. 42 (2003) 187–198.

[23] S.D. Hwang, I.H. Jang, H.H. Cho, Experimental study on flow and local heat/mass transfer characteristics inside corrugated duct, Int. J. Heat Fluid Fl. 27 (2006) 21–32.

[24] Y.S. Lee, C.C. Su, Y.M. Sun, J.C. Ye, Experimental study on heat transfer in wavy channels, J. Enhanc. Heat Trans. 10 (2003) 21–29.

[25] J.A. Stasiek, Experimental studies of heat transfer and fluid flow across corrugated-undulated heat exchanger surfaces, Int. J. Heat Mass Transfer 41 (1998) 899–914.

[26] G. Comini, C. Nonino, S. Savino, Effect of space ratio and corrugation angle on convection enhancement in wavy channels, Int. J. Numer. Method. H. 13 (2003) 500–519.

[27] M. Cabassud, C. Gourdon, intensification of heat transfer in chemical reactors: heat exchanger reactors, in: A. Cybulinski, J.A. Moulijn, A. Stankiewicz (Eds.), Novel Concepts in Catalysis and Chemical Reactors: Improving the Efficiency for the Future, WILEY-VCH Verlag GmbH & Co. KGaA, Weinheim, 2010, pp. 261–287.

[28] Y. Kato, Y. Tada, M. Ban, Y. Nagatsu, S. Iwata, K. Yanagimoto, Improvement of mixing efficiencies of conventional impeller with unsteady speed in an impeller revolution, J. Chem. Eng. Japan 38 (2005) 688–691.

[29] O. Levenspiel, Chemical reaction engineering, 3rd ed., John Wiley & Sons, New York, 1999, pp. 90–119.

[30] I.E. Idel'cik, in: E.D.F. Eyrolles (Ed.), Mémento des pertes de charges, 1986, p. 196.

[31] J. Zhang, J. Kundu, R.M. Manglik, Effect of fin waviness and spacing on the lateral vortex structure and laminar heat transfer in wavy-plate-fin cores, Int. J. Heat Mass Tran. 47 (2004) 1719–1730.

[32] R.K. Shah, A.L. London, Laminar flow forced convection in ducts, ed, Academic Press, New York, 1978, pp. 200–204.